JOURNAL OF MATERIALS SCIENCE **34** (1999) 2263–2267

Defect-induced microstructures: an X-ray diffraction analysis

J. CHROSCH*, M. COLOMBO
University of Cambridge, Department of Earth Sciences, Downing Street, Cambridge CB2 3EQ, UK

I. MEMMI, R. BIAGINI
University of Siena, Department of Earth Sciences, Via della Cerchia 3, I-53100, Siena, Italy

Single crystal X-ray diffraction was applied in order to investigate defect-induced microstructures in radiation damaged zircon. The formation of domains with different degrees of order was observed and in particular, it was possible to distinguish two types of defects: isolated lattice defects and dislocations. These lattice deformations have a great influence on the structural and physical properties of the materials. © *1999 Kluwer Academic Publishers*

1. Introduction

The presence and the distribution of defects clearly influence the physical properties of solid state substances and this effect is of great importance in all areas of materials science. The atomic arrangement in the unit cells of crystalline solids determines the properties of the bulk material under ambient conditions as well as their thermal, electric, magnetic and pressure dependent behaviour. However, the presence of defects can introduce microstructures and modify certain physical properties.

Recently developed high-resolution X-ray diffraction (XRD) facilities have already been shown to be ideally suited for the analysis of phase-transition-induced microstructures [1, 2]. These instruments combine a large number of rotational and translational degrees of freedom with position sensitive detectors in a way that there is no restriction in either size or orientation of the sample [2].

Diffuse as well as Bragg intensities are detected simultaneously using an area detector and are integrated within a suitable range around the Bragg reflections. If then plotted versus the respective angle of incidence (mainly ω, χ or φ, see Section 2) the results are usually referred to as XRD rocking curves [2].

In order to observe defect-induced microstructures we use a natural single crystal of zircon. This mineral occurs in various degrees of crystallinity depending on the amount of radiation damage it has suffered through α events and recoil damage due to the substitution of Zr mainly by U and Th [3–5].

The study of zircon is helped by its widespread presence as an accessory mineral in igneous, metamorphic and sedimentary rocks and by its comparatively simple tetragonal structure, which allows a rather straightforward structural interpretation of the damage mechanism [3, 4]. The damage is caused by two separate but simultaneous processes: firstly an α particle displaces several hundred atoms and generates mainly Frenkel defect pairs; and, secondly, recoil of the radiogenic atom produces clouds of several thousand atomic displacements [6]. The structural state of zircon is commonly characterized by the volume proportions of its following regions:

1. Regions of crystalline and essentially undistorted material that are equivalent to the undamaged zircon.
2. Regions of the crystalline but radiogenically damaged or distorted part.
3. Regions of aperiodic zircon (see [7]).

These regions are heterogeneously distributed due to the non-uniform distribution of radiogenic atoms [8, 9].

The aim of this study is the understanding of the radiation damage-induced microstructures in zircon, which has direct implications for the assessment of the applicability of zircon-type ceramics as potential host for radiogenic waste such as Pu, U, Th [5, 10–11].

2. Experimental procedure

For the diffraction experiments we used novel high-resolution instruments, which have been described in detail elsewhere [1, 2], and strictly monochromatic radiation (CuK_{α_1}).

To be able to observe the influence of an inhomogeneous distribution of the radiation damage a $20 \times 9 \times 6\,mm^3$ zoned single crystal of zircon was longitudinally scanned in its central position in 1 mm steps across the {1 0 0} face. In order to observe diffuse scattering from the radiation-induced microstructures in the

* New permanent address: The Robert Gordon University, Applied Sciences, St. Andrew Street, Aberdeen AB25 1HG, UK.

crystal the (2 0 0) Bragg reflection was chosen and the angle of incidence, ω, was varied over a comparatively large range (10°) with a counting time of 1200 s per step.

The rocking curves were then constructed by integrating a certain "region of interest" of each spectrum with respect to the tilt angle, yielding integrated intensities versus ω.

3. Results

XRD was used to investigate the structural state of the zircon single crystal. The (2 0 0) reflection was chosen in order to extrapolate the best results because of its high structure factor. Farges [12] reported that this signal remains visible in highly amorphized zircon even when the other Bragg reflections have disappeared from the powder diffraction pattern.

The procedure of characterizing the defect-induced microstructures in a single crystal involves: (i) identification of the type of defects, i.e. interstitials, vacancies, dislocations, prevailing in a given region; and (ii) the orientation of this region with respect to the matrix, i.e. mosaicity.

Fig. 1 shows the ideal cases of diffraction patterns as observable on a two-dimensional detector for either a single crystal (Fig. 1a), a randomly oriented powder sample (Fig. 1b) and a sample with some degree of mosaicity (Fig. 1c). We define a *single crystal* as a defect-free sample, if the full-width-at-half-maximum (FWHM) of its rocking curves with respect to any of the relevant angles (ω, χ, 2θ) are of the order of 0.01°, and, in particular, if their respective ratios are equal to one [2].

In a *randomly oriented powder sample* the width in 2θ varies according to the grain size and is typically of the order of 0.1°. Along the χ cones there is an equal intensity distribution, which is usually referred to as a powder line. It is, in general, not possible to construct rocking curves from a powder sample. A *defective crystal* represents an intermediate case whose diffraction pattern requires a careful analysis.

In our zircon sample the observed (2 0 0) peaks are generally broadened when compared with the signal from an ideal single crystal, indicating that it is indeed a sample with some degree of radiation damage. Scanning across the crystal allows us to distinguish the structural inhomogeneities and to characterize the present lattice distortions.

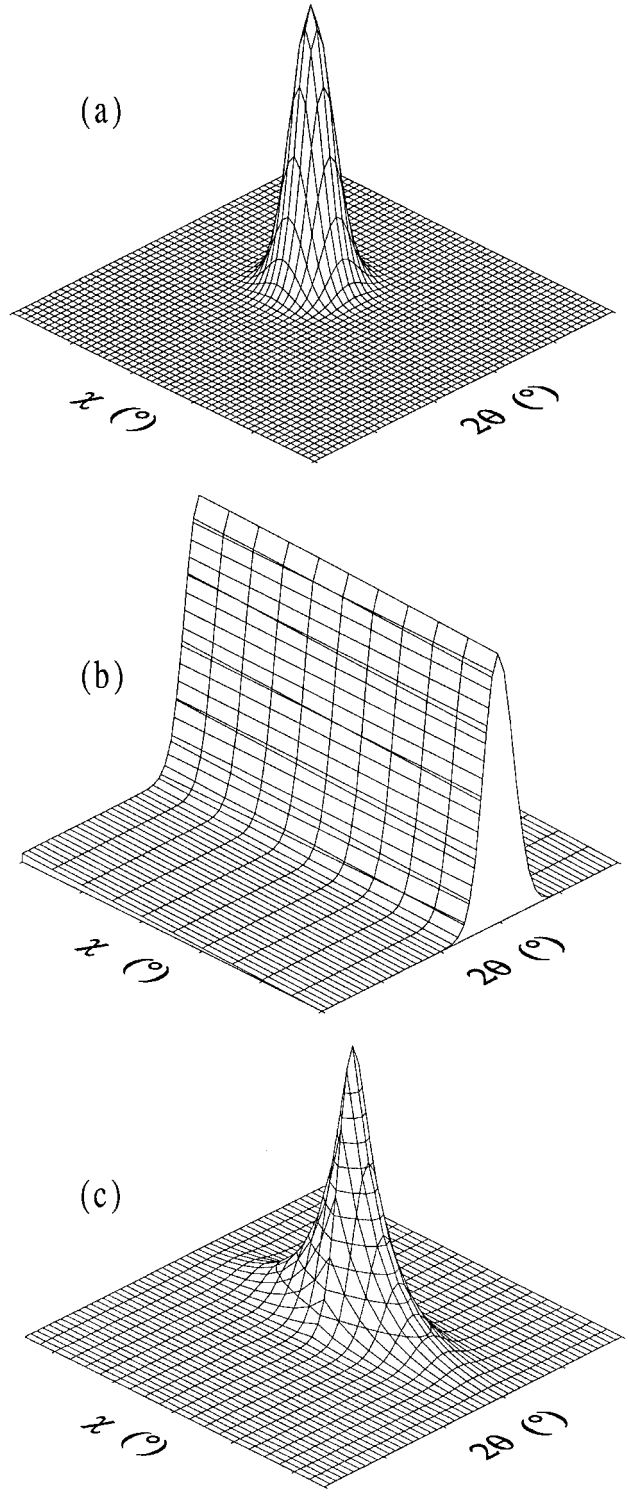

Figure 1 Examples of diffraction patterns for (a) a single crystal, (b) a randomly oriented powder sample, and (c) a sample with some degree of mosaicity.

3.1. Gaussian line fitting

In the first instance, all reflections in all three directions are fitted with two Gaussian curves.

3.1.1. 2θ direction

Fig. 2 shows the distribution of the peak positions at the different scanning points for the peak (G1) and the background (G2). The distribution of the G1 points is quite constant around the value $2\theta = 26.95°$; peak No. 10 is at higher 2θ and its deviation from the average value is considerably larger than the one expected from statistical noise only. The G2 values are more scattered, in particular, point No. 2 is very close to the G1 value, indicating that it is necessary to use three curves in order to take into consideration the high diffuse scattering contribution at lower 2θ angles. Fig. 2 shows the results of the peak analysis using three curves. While the position of the main peak is now consistent with the other datum point, lower angle scattering is centred at $2\theta = 26.83°$. G2 points more separated from the

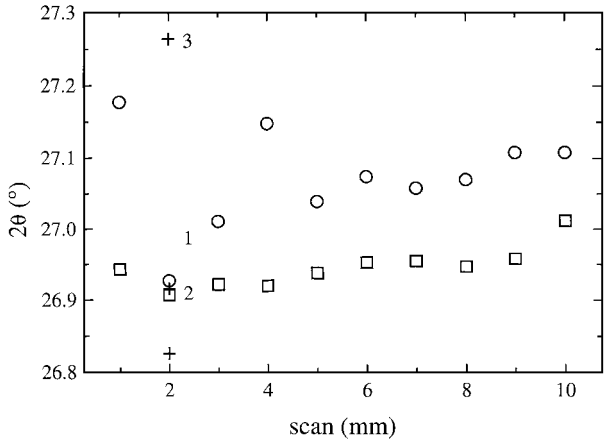

Figure 2 Distribution of the peak positions in the 2θ direction at different scanning points for the peak (□) and for the background (○). The crosses refer to peak analysis of point No. 2 using three curves: (1) main peak, (2) diffuse scattering at lower 2θ and (3) background.

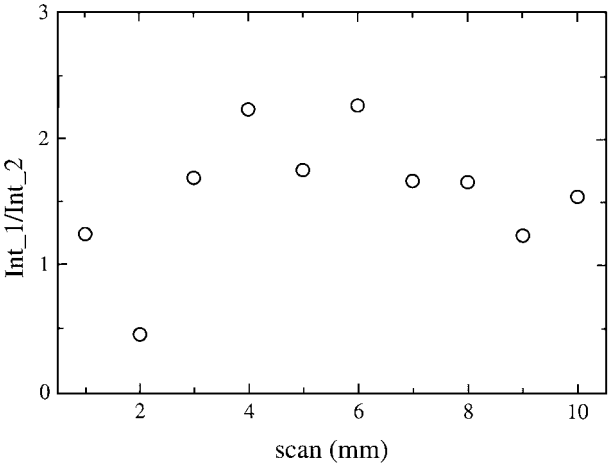

Figure 3 Ratio of the integrated intensities of the peak (Int_1) and of the background (Int_2) in the 2θ direction.

G1 points indicate that the curve indeed fits just the background.

The ratio between the intensity of the peak (G1) and of the background (G2) is quite constant around 1.6 (Fig. 3).

The line broadening, described as FWHM, of the G1 peaks is also not too scattered around an average of 0.21°. Peaks No. 9, 10 and 2 (three-curve fitting) are therefore definitely much broader (Fig. 4).

3.1.2. χ direction

A similar analysis of the observed profiles of the (2 0 0) peak in the χ direction shows scattered values of the peak positions (Fig. 5), while the intensity ratio is almost constantly equal to one. This ratio is much higher for peaks No. 5 and 6 because they are more symmetric.

The line broadening data are instead scattered (Fig. 6). Notice, that the average FWHM value is 1.40°, which is much larger than the average FWHM observed in the 2θ direction (0.21°). The widths of peaks No. 2, 7 and 10 are smaller compared with the others because of the asymmetric distribution of the intensity, which results in the presence of two sharper peaks (G2 data, Fig. 6).

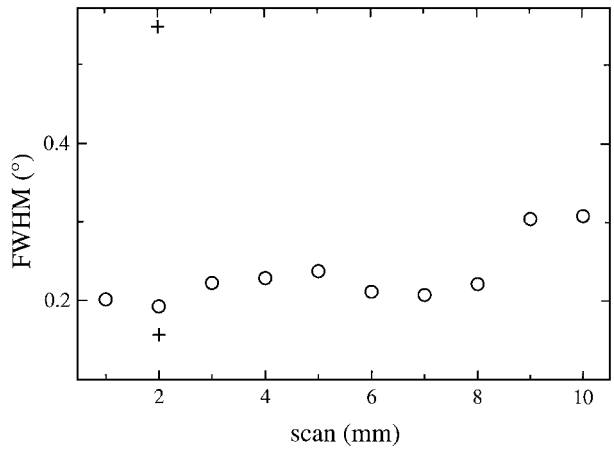

Figure 4 Line broadening, described as FWHM, for G1 peaks (○) in the 2θ direction. The crosses (+) refer to peak analysis of point No. 2 using three curves.

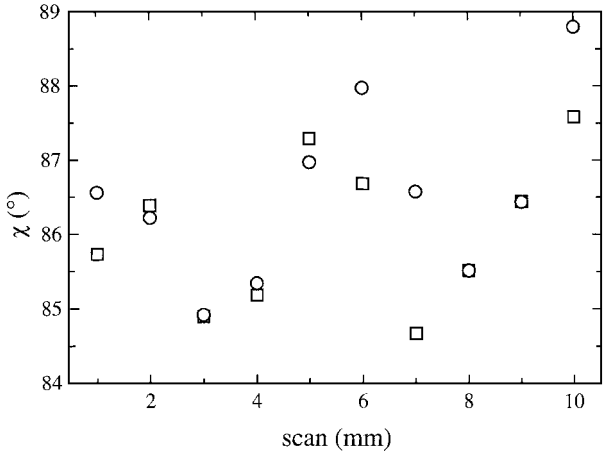

Figure 5 Distribution of peak positions in the χ direction at different scanning points for the peak (□) and for the background (○).

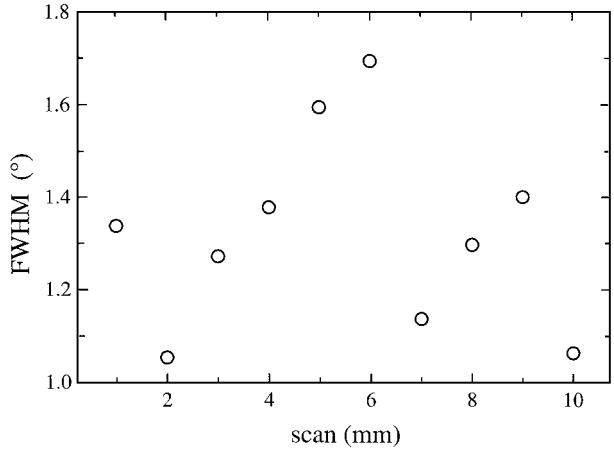

Figure 6 Line broadening, described as FWHM, for peaks in the χ direction.

3.1.3. ω direction

Peak positions in the ω direction are quite scattered (Fig. 7) and so are both the intensity ratio (Fig. 8) and the FWHM values (Fig. 9), although 1° can be chosen as an average value for the broadening in this direction.

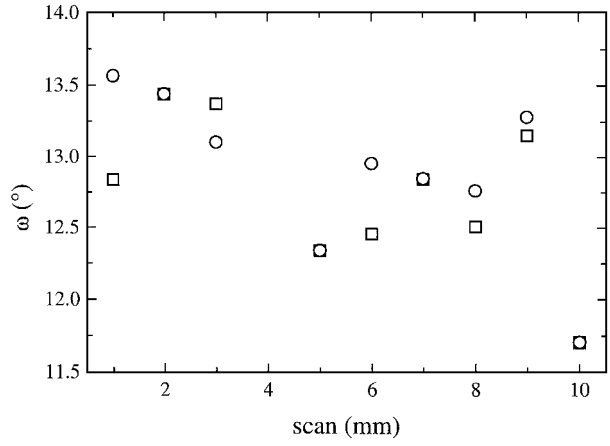

Figure 7 Distribution of peak positions in the ω direction at different scanning points for the peak (□) and for the background (○).

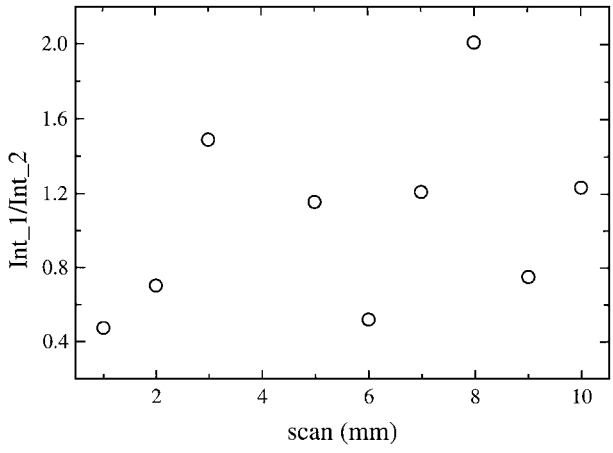

Figure 8 Ratio of the integrated intensities of the peak (Int_1) and of the background (Int_2) in the ω direction.

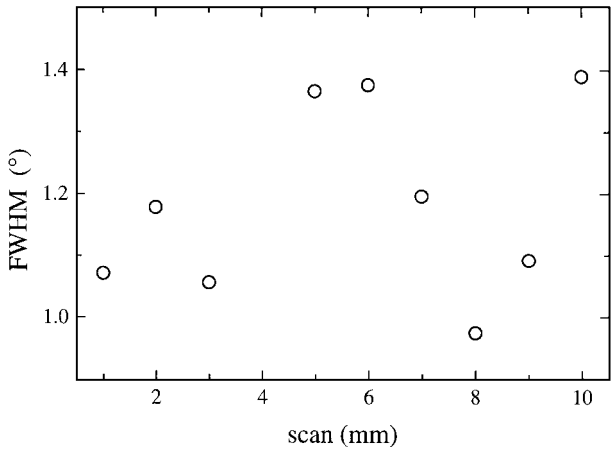

Figure 9 Line broadening, described as FWHM, for peaks in the ω direction.

3.2. Peaks deviating from average behaviour

From these observations it is possible to identify peaks No. 2, 6 and 10 as the ones deviating from average behaviour. Therefore, a more detailed description of these peaks follows.

3.2.1. Peak No. 2

This peak is one of the sharpest in the χ direction, indicating a low degree of mosaic spread, while it is very broadened in the 2θ direction, where diffuse scattering, at low 2θ with respect of the Bragg peak, is dominant with an integrated intensity 1.9 times the one of the Bragg peak. In the ω direction there are no main deviations from average behaviour.

3.2.2. Peak No. 6

This peak is so asymmetric in the ω direction that it will be better fitted using three curves instead of just two. In this way, the diffuse scattering (background excluded) has an integrated intensity of approximately six times the one of the main peak and a width of 3.2°, which is considerably broader than the ones in all other directions.

3.2.3. Peak No. 10

This peak is asymmetric and broadened in all directions.

4. Discussion

Single crystal XRD analysis of a highly defective and inhomogeneous phase [13, 14], such as radiation damaged zircon, allows observation of domains with different structural states (microstructures). In particular it is possible to distinguish two main types of defects: (i) isolated defects [15, 16] related to α-particles radiation and their contribution to the formation of strained domains with expanded lattices; and (ii) dislocations [16–18].

4.1. Isolated defects

The simplest structural imperfections in solids are those involving single lattice points. A Frenkel defect results when the displaced atom is lodged in an interstitial site in the lattice. The total volume change produced by the presence of n defects (i.e. interstitial atoms and vacancies) to N atomic sites is $\Delta V/V = n/N + (\Delta V/V)_e$, where $(\Delta V/V)_e$ is the volume change due to elastic strain caused by evenly distributed point defects and is simply that which would be given by homogeneous dilatation $(\Delta V/V)_e$ [19].

In the diffraction pattern the resulting diffraction signal is broadened in the 2θ direction by the presence of diffuse scattering in the low-2θ side of the Bragg peak. For example, peak No. 2 can be deconvoluted into two components: the Bragg peak at $2\theta = 26.92°$ and diffuse scattering at $2\theta = 26.83°$. The lattice strain is $e_1 = \Delta a/a_0 = 0.03$, where Δa is the difference between the value of the lattice parameter a calculated using the diffuse scattering position and the value a_0 calculated using the Bragg peak position. The measured lattice strain is indeed in good agreement with the values expected for volume expansion induced by α-particle damage [5, 15].

4.2. Dislocations

It is obvious that the defect with the lowest energy of formation will predominate. The simple defect configuration of isolated Frenkel defects is not necessarily the most stable structure. For example, a pair of closely associated vacancies might have a lower energy than the two defects considered separately. Detailed computer calculations have led to a number of interesting configurations for point defect complexes involving three and four vacancies [19]. Under certain conditions, e.g. irradiation, a large supersaturation of point imperfections may exist and it may lead to a more extensive form of defect aggregation. Dislocation lines may be produced under extreme conditions when point defects coagulate on some atomic plane to form a sheet or disc of point defects [19].

In the diffraction pattern the resulting diffraction signal when dislocations are present is widely broadened in the direction perpendicular to the dislocation line and some broadening is observed in both the 2θ direction, because of dislocation-induced lattice strain, and in the χ direction, because of small angle tilt between adjacent domains [18, 20]. Our experiment is set such that the diffuse scattering induced by the dislocations is observed parallel to the ω direction. In order to be sure that this diffuse scattering is indeed due to dislocations and not just a high degree of grain misorientation we compare the FWHMs measured in the ω and χ directions. For example, peak No. 6 clearly shows a more pronounced peak broadening in ω than in the other two directions, indicating the presence of dislocations. Knowing the Burger's vector it is possible to estimate the dislocation density by measuring peak broadening in the ω direction.

Together with the effects related to the presence of these two main types of defects it is possible to observe how a higher degree of radiation damage influences the diffraction signal (peak No. 10), both exacerbating the previously indicated effects, i.e. superimposing dislocation-related strain broadening to elastic strain broadening (isolated defects) and shifting the peak position in the 2θ direction towards higher values, indicating the presence of amorphous material compressing the damaged phase.

5. Conclusions

The presence of defect-induced microstructures was observed with single crystal XRD. It was possible to distinguish two types of dominant defects: isolated defects and dislocation lines.The former manifest themselves as line broadening in the 2θ direction. An estimate of the lattice strain induced by volume expansion is obtained using the position of the Bragg peak and of the diffuse scattering component. The dislocations account for a general broadening of the reflection but with a stronger effect on the direction perpendicular to the dislocation line. Their presence is therefore best envisaged calculating the peak eccentricity.

The possibility of observing the presence of dislocations using XRD is of great importance in all areas of materials science, in fact, almost any sample is suitable for characterization without the need to be, for example, ion-thinned for transmission electron microscopy or polished for X-ray topography.

Acknowledgements

This work was supported by British Nuclear Fuel Liquids.

References

1. J. CHROSCH and E. K. H. SALJE, *Ferroelectrics* **187** (1996) 1.
2. J. CHROSCH *et al*., *Physica C* **265** (1996) 233.
3. H. D. HOLLAND and D. GOTTFRIED, *Acta Crystallogr.* **8** (1955) 291.
4. T. MURAKAMI *et al*., *Adv. Ceram.* **20** (1986) 745.
5. R. C. EWING *et al*., *J. Mater. Res.* **10** (1995) 243.
6. W. J. WEBER, *J. Nucl. Mater.* **98** (1981) 206.
7. T. MURAKAMI *et al*., *Amer. Mineral.* **76** (1991) 1510.
8. P. E. FIELDING *et al*., *ibid.* **55** (1970) 428.
9. J. CARPENA *et al*., *Bull. Mineral.* **110** (1987) 459.
10. A. B. HARKER and J. F. FLINTOFF, *J. Amer. Ceram. Soc.* **68** (1985) 159.
11. *Idem, ibid.* **73** (1990) 1901.
12. F. FARGES, *Phys. Chem. Minerals* **20** (1994) 504.
13. S. ELLSWORTH *et al*., *ibid.* **21** (1994) 140.
14. L. A. BURSILL and A. C. MCLAREN, *Phys. Status Solidi* **13** (1966) 331.
15. W. J. WEBER, *J. Amer. Ceram. Soc.* **65** (1982) 544.
16. K. YADA *et al*., *Phys. Chem. Minerals.* **14** (1987) 197.
17. M. COLOMBO and J. CHROSCH, *Radiation Phys. Chem.* **53** (1998) 555.
18. V. M. KAVANER *et al*., *Phys. Rev.* **B55** (1997) 1793.
19. B. HENDERSON, in "Defects in Crystalline Solids" (Edward Arnold, London, 1972) p. 27.
20. W. A. WOOLFSON, in "Diffuse X-Ray from Crystals" (Dover Publications, New York, 1997).

Received 20 July
and accepted 28 August 1998